IEEE Access
Multidisciplinary ⋮ Rapid Review ⋮ Open Access Journal

Received April 12, 2021, accepted April 27, 2021, date of publication April 30, 2021, date of current version May 10, 2021.

Digital Object Identifier 10.1109/ACCESS.2021.3076781

Wireless Telecommunication Links for Rainfall Monitoring: Deep Learning Approach and Experimental Results

FEYISA DEBO DIBA[1,2], MD ABDUS SAMAD[1,3], (Graduate Student Member, IEEE), JIWAN GHIMIRE[1], AND DONG-YOU CHOI[1], (Senior Member, IEEE)

[1]Department of Information and Communication Engineering, Chosun University, Gwangju 61452, South Korea
[2]Department of Electronics and Communication Engineering, Adama Science and Technology University, Adama 1888, Ethiopia
[3]Department of Electronic and Telecommunication Engineering, International Islamic University Chittagong, Chattogram 4318, Bangladesh

Corresponding author: Dong-You Choi (dychoi@chosun.ac.kr)

This work was supported in part by the Framework of International Cooperation Program managed by the National Research Foundation of Korea under Grant NRF-2020K2A9A1A09095712, and in part by the Brain Korea 21 Four Program through the National Research Foundation of Korea (NRF) by the Ministry of Education under Grant 4299990114316.

ABSTRACT Recently, wireless telecommunication networks have become a promising alternative for rainfall measuring instruments that complement existing monitoring devices. Due to big dataset of rainfall and telecommunication networks data, empirical computational methods are less adequate representation of the actual data. Therefore, deep learning models are proposed for the analysis of big data and give more accurate representation of real measurements. In this study, we investigated rainfall monitoring results from experimental measurements and deep learning approaches such as artificial neural networks and long short-term memory. The experimental setups were in South Korea over terrestrial and satellite links, and in Ethiopia over terrestrial link for different frequency bands and link distances. The received signal level and rainfall data measurement covered four years in South Korea and the data were sampled at intervals of 10 seconds. In Ethiopia, the data were recorded over 10 months and sampled at intervals of 15 minutes. The received signal power data were used to derive the rainfall rate distribution and compared to actual rainfall measurements over the same time periods. Our results demonstrate that the proposed deep learning-based models generally have a good fit with the measured rainfall rates. The rainfall rate generated from terrestrial links was a better fit to the actual rainfall rate data than that generated from satellite links.

INDEX TERMS LSTM, rainfall monitoring, artificial intelligence, deep learning, received signal level, South Korea, Ethiopia.

I. INTRODUCTION

Precise and real-time precipitation observations play a significant role in various aspects of human life, such as hydrometeorology, agriculture, climate monitoring, and natural disaster warning. Currently, rainfall monitoring methods include weather radar, rain gauges, and weather satellites [1], [2]. The rain gauge (RG) is used as an accurate ground-based rainfall estimation instrument. However, it does not provide rainfall information with high spatial resolution owing to errors introduced by calibration or ground winds [3]–[5]. The weather radar can address the shortcomings of the RG and provide a wide range of precipitation distribution information, but ground clutter frequently affects it, which results in less accurate ground-level observations [6]. In the South Korean context, the radar monitoring network operated by the Korea Meteorological Administration has a comparatively high density and is mounted at positions suitable for observations of the peninsular part of the country. Nevertheless, it has limited representation in urban areas [7]. Therefore, it is imperative to develop real-time, accurate, and representative rainfall measurement techniques.

Recently, wireless telecommunication links have gained attention as a promising rainfall measurement method because the power of received signals, which is extremely sensitive to rainfall in microwave and millimetric frequency bands, can be measured everywhere for communications [8]–[11]. Several studies have shown the potential application

The associate editor coordinating the review of this manuscript and approving it for publication was Guido Valerio.

of terrestrial radio links for rainfall prediction in different parts of the world over several different carrier frequencies (5–50 GHz) [12]–[16]. Outstanding examples are the nationwide campaign in Germany [17] and the Netherlands [18], which confirmed that commercial microwave links (CML) can provide precipitation data that correspond well with gauge and weather radar rainfall information

Rainfall data derived from the telecommunication signal were successfully applied to the simulations of river runoff in Germany for a pre-alpine catchment area [19], [20], and for small urban catchment pipe flow simulation in the Czech Republic [21]. Furthermore, the first CML-derived rainfall generation in a developing country was carried out by [22], using CML data from Burkina Faso.

More interestingly, with the rollout of 5G wireless networks, relevant research has indicated that densely distributed terrestrial links can measure rainfall in urban areas either as a primary or supplementary precipitation monitoring method [23]–[27]. In addition to terrestrial links, it is also possible to successfully retrieve rain rates from the signal level received from satellite links, as seen in the Paris area [28]. Many studies have also shown that dense commercial earth-space links are potential global high-resolution rainfall monitoring systems [29]–[31].

Several telecommunication-derived rainfall measurement algorithms have been developed by researchers. The first rain event detection method presented in [32] was based on the rolling standard deviation threshold for time series attenuation. This technique has also been used in recent studies [7], [17], [33] such as one that developed Fourier transformations on a rolling window to detect rain event patterns in the frequency domain [34].

Another article [35] applied a Markov switching model that used Gaussian factor graphs and random forest classifiers [36]. It applied a simple multi-layer perception [36] and in [37] proposed a rolling mean method for dynamic baseline determination.

Currently, deep learning is a fast-evolving field for modeling different physical phenomena from data, mainly when big data needs to be processed [38]. Considering rainfall derived from communication links, deep learning techniques [39] have been applied to separate wet and dry periods using satellite communication data to optimize rainfall retrievals, and the study [19], [40] implemented a machine learning approach for dry-wet classification from commercial microwave links. Few other studies have applied deep learning to rainfall-runoff modeling [41], [42]. Most of the existing studies are based on the classification of rainfall as dry and wet. Therefore, in this study we address the generation of rainfall events, the amount of rainfall produced over the year, and estimate the duration of rainfall events from experimental and deep learning models.

This study makes the following contributions:

- To the best of our knowledge, this study is the first wireless telecommunication-based rainfall monitoring system in South Korea and Ethiopia in these frequency bands. The retrieval of rainfall data from wireless communication links has been investigated in South Korea over four terrestrial line-of-sight links and two satellite networks, and over one terrestrial line-of-sight at microwave frequency spectrum link in Ethiopia.
- The experimental rainfall rate distribution statistical results from the measured rain data were compared with the rain rate produced by the two proposed deep learning models. The analysis shows that the long short-term memory (LSTM) model provides a more accurate estimate than a simple artificial neural network (ANN). Moreover, the past studies have been mainly wet-dry periods classification, however, our study deals with the generation of rainfall at every level and comparing the distribution over the year.
- This study is mainly based on the actual received signal power and rain rate data measurements, which make the findings practically sound.
- While deep learning in many main fields has achieved several milestones, but the black box aspect of deep learning impedes its comprehension significantly because of its nonlinear nature. As a result, this study attempts to unravel every black box in the deep learning networks that have been introduced.

This paper is organized as follows: Section II provides an overview of the experimental set up over three sites. Section III provides detailed information on the proposed deep learning models, and Section IV discusses the results obtained from the experimental results and proposed models. The conclusions are presented in Section V.

II. EXPERIMENTAL SETUP

This study addresses three experimental scenarios such as terrestrial links in South Korea, satellite links in South Korea, and terrestrial microwave links in Ethiopia. The impact of different network factors such as operational frequencies, geographical locations, and link distances, on rainfall monitoring over the various links is analyzed in these experiment.

A. TERRESTRIAL LINKS MEASUREMENT CAMPAIGN IN SOUTH KOREA

The terrestrial experimental networks were established in Icheon, South Korea, between the Khumdang tower (37.135669°N 127.5156°E, Korea Telecom, KT station) and the Icheon tower (37.147103°N 127.548561°E, National Radio Research Agency, (RRA) station) for rainfall rate and received signal power measurements at interval time of 10-seconds.

The above link has a 3.2 km path length and operates at 18 GHz with horizontal and vertical polarization and 38 GHz carrier frequencies with vertical polarization. Similarly, the E-band (75 GHz) link is between the same Icheon tower and EMS Dong Yoksang station (37.197°N 127.426°E), at a link distance of 0.1 km. The received signal power and rain rate data were simultaneously collected at the receivers over four years over the above links. The

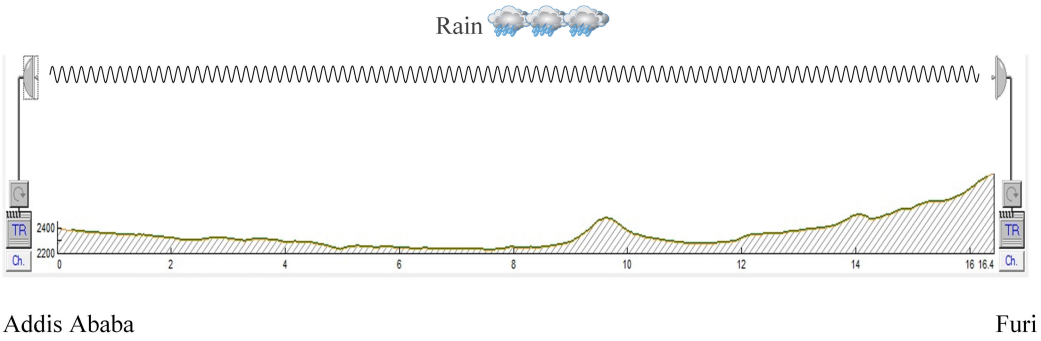

FIGURE 1. Back-haul microwave link between Furi and Addis Ababa, Ethiopia.

detailed link profile and the experimental setups are given in [43], [44].

B. SATELLITE LINKS MEASUREMENT CAMPAIGN IN SOUTH KOREA

The RRA installed a satellite link experimental setup at the building of the Radio Promotion Association (37.545903°N 126.883°E) Dong-13 na-gil, Yangcheon-gu, Seoul, Republic of South Korea. The beacon receiver measures the received signal level power in the 12.25 and 20.73 GHz frequency bands of the Korea Sat-6 satellite with an antenna diameters of 1.8 m. The detailed rainfall, received signal power measurements, and link profile specifications are given in [45].

C. TERRESTRIAL LINK IN ETHIOPIA

Experimental data collection of the received signal level for the terrestrial line-of-sight link between Furi and Addis Ababa was conducted in collaboration with Ethio-telecom at a 15-minute sampling rate. Records for the minimum, average, and maximum values were collected. The link is vertically polarized at an operating frequency of 11 GHz and path length of 16.42 km. Measurements were taken over a period of ten months between 2015 and 2016. The data collection was based on the existing terrestrial link set up between Addis Ababa (08.52582°N, 38.41125°E as the receiving (Rx) site and Furi (09.01067°N, 38.44504°E as the transmitting (Tx) station. The heights provide sufficient clearance, as seen in the path profile in Fig. 1, and detailed link parameters for the radio propagation network are also provided in Table 1. In addition to the received signal power measurements of the link, raw rainfall data were collected by the National Meteorological Agency of Ethiopia at intervals of 15 min for the same period of the received signal level for target training and validation of the deep learning algorithms.

The expected received signal power $P_r(t)$ is computed using the following formula:

$$P_r(t) = P_t(t) + G_t(t) + G_r(t) - FSL - A_t \quad (1)$$

where $P_t(t)$ is the power from the transmitter usually expressed in terms of dBm; A_t is the total attenuation loss due to atmospheric gases, vegetation, buildings, clouds, rain, and fogs: $G_r(t)$ is the receiver antenna gain; $G_t(t)$ is the transmitter antenna gain: FSL is the free space path loss.

TABLE 1. Link profile parameters for microwave link in Ethiopia.

Parameters	Furi (Tx)	Between	Addis Ababa (Rx)
Elevation (m)	2401		2842
Latitude	09.01067°N		08.52582°N
Longitude	038.44504°E		38.41125°E
Antenna gain (dBi)	42		42
Antenna height (m)	10		10
Tx line unit loss(dB/100)	4.53		4.53
Tx line loss(dB)	0.91		0.91
Frequency (GHz)	11		11
Circuit branching loss (dB)	6.8		6.8
True azimuth (°)	203.92		23.91
Vertical angle (°)	1.48		-1.59
Link length (km)		16.42	
Free space loss (dBm)		139.6	
Tx power (dBm)		30	
Frequency spacing (MHz)		21.7	
Rx threshold level (dBm)		-76.2	
Atmospheric absorption (dB)		0.35	

$$A_t = A_{\text{rain}} + A_{\text{no-rain}} \quad (2)$$

$$A_{\text{rain}} = A_t - A_{\text{no-rain}} \quad (3)$$

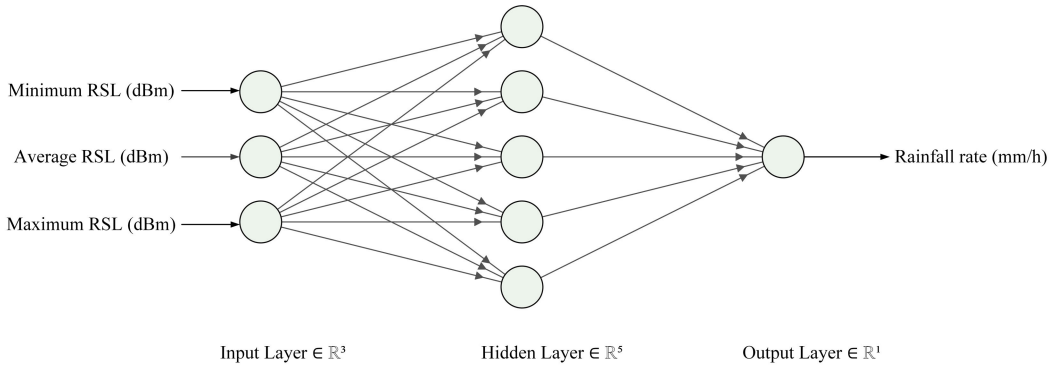

FIGURE 2. Rainfall rate prediction based on artificial neural network model, where RSL is the received signal level.

where A_{rain} and $A_{no\text{-}rain}$ represent attenuation induced by rain and attenuation from any other than, rainfall conditions, respectively.

III. DEEP LEARNING

Artificial intelligence (AI) is transforming the world by influencing every human being in every industry. It is the main driver of emerging technologies like robotics, big data, and IoT to enables human to rethink how we analyze data, integrate information, and use the results for optimum decision-making. Deep learning is an AI that consists of computational models composed of several processing layers that learn features of data through multiple layers of networks, using forward and backward propagation algorithms. ANN, convolutional neural networks, and recurrent neural networks (RNN), are types of deep learning. In this study, we implement ANN and RNN models for rainfall monitoring from received signal levels of terrestrial and slant links in South Korea operating at several frequency bands, and microwave link in Ethiopia.

A. ARTIFICIAL NEURAL NETWORK

An ANN is an intelligent system used for solving complicated problems in several applications such as prediction, optimization, modeling, simulation, pattern recognition, clustering, and others. Several experiments show that an accurate prediction can be achieved by using the ANNs [46], [47]. As shown in Fig. 2, the ANN consists of three layers: the input layer which collects data, one or more hidden layers used to connect the input and output layers and, an output layer that gives computed information. A neuron is the fundamental processing unit of ANN which performs the collection of the inputs and production of the output. Each input is multiplied by connection weights, and added to biases then passed through an activation function to get an output results using forward pass. The predicted outputs achieved based on the input data from the input layers are then compared with the target output. The error between predicted and target outputs is obtained at the end is then propagated to the input layer through backward propagation to update the ANN parameters for optimum results [48].

In this study, we used an ANN with three input layers equivalent to the dimensions of the input features, such as the minimum, average, and maximum received signal levels, as well as one hidden layer consisting of five nodes and a single output layer, as shown in Fig. 2. The dimensions of the hidden nodes are determined using the general principle, in which the number of hidden neurons is less than twice the number of input layers [49], [50].

An ANN is a model of activation function R_j with the input $S = (S_1, S_2 \ldots, S_L)$ multiplied by a vector of weights $\omega_j = (\omega_{j1}, \omega_{j2} \ldots, \omega_{jL})$ plus a node bias β_j.

With an ANN, the forward pass maps the input information S_i to the target output O through the hidden layer. The mathematical equations for the forward pass are as follow [51], [52].

$$T^{[n]} = \omega^{[n]T} R^{[n-1]} + \beta^{[n]}, \quad 1 \le n \le N \tag{4}$$

$$R^{[0]} = S_i \tag{5}$$

$$R^{[n]} = \frac{1}{1 + exp(-T^{[n]})}, \quad 1 \le n \le N \tag{6}$$

where $R^{[n]}$, N, and $T^{[n]}$ are activation functions, the overall amount of layers, and the transformations on the n^{th} layers, respectively, and the transformation parameters are given as $\omega^{[n]}$ and $\beta^{[n]}$ for n layers.

Back propagation has been used to minimize the errors between the observed and expected results. Backward propagation transfers the weight of the forward pass function from the output "O" to the input "S_i" in neural networks. The loss function $L(O, R)$ was implemented to evaluate the discrepancy between the computed output 'R' and target output "O". The mean real squared error regression analysis was applied to the loss function as follows: [53]:

$$L(O, R) = \frac{1}{2m} \sum_{m=1}^{m} (|O - R|^2) \tag{7}$$

In this study, "0," "1," and "2," are used to represent the input, hidden, and output layers, respectively. The number of units is three, five and one for the input, hidden, and output

layers, respectively. For our proposed models, the data were split into 85% and 15% for training and testing, respectively. The Korean data contain 3 × 216 480 sample-input received signal level elements and 2164 800 samples of the target rainfall rate. As shown in Fig. 2, we developed three input feature elements: minimum, average and maximum received signal levels, and five nodes in the hidden layer. Thus, the bias of the ANNs is $\beta^{[1]}$, the transformation $T^{[1]}$, the weights of the ANN inside the hidden layer are (5, 3), and the result of hidden layer $R^{[1]}$ vectors are (5, 1). The transformation $T^{[2]}$ and the final result $R^{[2]}$ are (1, 1) vectors which can be mathematically presented as:

$$\begin{bmatrix} T_1^{[1]} \\ T_2^{[1]} \\ \vdots \\ T_5^{[1]} \end{bmatrix} = \begin{pmatrix} \omega_{1,1}^{[1]} & \omega_{1,2}^{[1]} & \omega_{1,3}^{[1]} \\ \omega_{2,1}^{[1]} & \omega_{2,2}^{[1]} & \omega_{2,3}^{[1]} \\ \vdots & \ddots & \vdots \\ \omega_{5,1}^{[1]} & \omega_{5,2}^{[1]} & \omega_{5,3}^{[1]} \end{pmatrix} \begin{bmatrix} s_1 \\ s_2 \\ s_3 \end{bmatrix} + \begin{bmatrix} \beta_1^{[1]} \\ \beta_2^{[1]} \\ \vdots \\ \beta_5^{[1]} \end{bmatrix} \tag{8}$$

$$R^{[1]} = \begin{bmatrix} R_1^{[1]} \\ R_2^{[1]} \\ \vdots \\ \alpha_5^{[1]} \end{bmatrix} \tag{9}$$

$$\left[\, T^{[2]} \right] = \begin{bmatrix} \omega_{1,1}^{[2]} & \omega_{1,2}^{[2]} & \omega_{1,5}^{[2]} \end{bmatrix} \begin{bmatrix} \alpha_1^{[1]} \\ \alpha_2^{[1]} \\ \vdots \\ \alpha_5^{[1]} \end{bmatrix} + \left[\, \beta^{[2]} \right] \tag{10}$$

$$R^{[2]} = \frac{1}{1 + exp(-T^{[2]})} \tag{11}$$

where $\omega_{\mathrm{jn}}{}^{[1]}$ denotes weights of the hidden layers, $\omega_{\mathrm{jn}}{}^{[2]}$ represent the weights of the output layers, and $\beta_{\mathrm{j}}{}^{[1]}$, $\beta_{\mathrm{j}}{}^{[2]}$ are the biases. The $\mathrm{T_j}^{[1]}$ vector indicates the input to the output layer, and $\mathrm{T_j}^{[2]}$ shows the results of the forward transmission.

Once the inputs have been transmitted to the outputs through the forward pass, the target output is compared with predicted output and then the error value is evaluated, finally parameters such as bias and weight are updated through reverse propagation to obtain optimum performance [54]. The stochastic gradient descent function is applied to update the weights and biases of the networks, as given in the following equations:

$$\omega^{[n]} += \omega^{[n]} - kd\omega^{[n]}, \quad 1 \le n \le N \tag{12}$$

$$\beta^{[n]} += \beta^{[n]} - kd\beta^{[n]}, \quad 1 \le n \le N \tag{13}$$

where $\omega^{[n]}$ and $\beta^{[n]}$ denote the weight and bias matrices, respectively, while $\omega^{[n]}+$ and $\beta^{[n]}+$ represent the update of weight and bias matrices, respectively. $d\omega^{[n]}$ and $d\beta^{[n]}$ are the derivatives of the weight and bias, respectively, while k indicate the learning rate.

The derivation of the loss function is a measure of rate of change of the loss function based on the variation in its input value. Moreover, the gradient shows the level to which the input parameters need to vary in order to minimize the losses, as given below:

$$dT^{[n]} = \frac{\partial L(O, R^{[n]})}{\partial T^{[n]})} = R^{[n]} - O, \quad 1 \le n \le N \tag{14}$$

$$d\omega^{[N]} = \frac{\partial L(O, R^{[N]})}{\partial T^{[n]})} \frac{\partial T^{[n]})}{\partial \omega^{[n]})} = dT^{[n]} R^{[n]'}, \quad 1 \le n \le N \tag{15}$$

$$d\beta^{[n]} = \frac{1}{m} dT^{[n]}, \quad 1 \le n \le N \tag{16}$$

$$dT^{[n-1]} = d\omega^{[n]'} dT^{[n]} g^{[n]}(^{[n]}), \quad 1 \le n \le N \tag{17}$$

B. LONG SHORT TERM MEMORY (LSTM)

LSTM is a special type of RNN with memory structures that are well-known for learning long-term data. When dealing with long-term dependencies, traditional ANNs do not relate previous information to the current time steps. However, LSTM was developed to overcome these issues [55], [56]. In this study, we considered the standard LSTM, widely applied for sequence-to-sequence modeling with long-term memory. This maps the input features $x(t)$ to the output prediction $h(t)$ from forward pass through a number of hidden variables that have many functions. This is to model past dependencies of the dataset as illustrated in Fig. 3. The LSTM gate variables of the networks are the forget gate $f(t)$, input gate $i(t)$, candidate vector gate $v(t)$, output gate $o(t)$, hidden layer $h(t)$, and memory cell state $c(t)$ [57], [58]. The forget gate removes out unwanted data from the memory whereas the input gate determines whether the present incoming data is provides new information to the network, and the output gate decides what to output. The derivations of the forward and backward propagation of our LSTM model are discussed in the next section.

1) FORWARD PROPAGATION

The activation functions of the forget gate, the input gate and output gate are implemented using a sigmoid function whereas the candidate vector gate which updates the cell state vector is realized using the tanh function. These activation functions are determined using the following equations for the forget gate T_f, input gate T_i, candidate gate T_v, output gate T_o, cell state C_t, and predicted output h_t. In addition, we have simplified the notation of the *tanh* and the *sigmoid* function using the symbols $\mathbb{T}$ and $\mathbb{S}$, respectively.

$$T_f = w_{fx} \cdot x_t + w_{fh} \cdot h_{t-1} + b_f \tag{18}$$

$$R_f = \mathbb{S}(T_f) \tag{19}$$

$$T_i = w_{ix} \cdot x_t + w_{ih} \cdot h_{t-1} + b_i \tag{20}$$

$$R_i = \mathbb{S}(T_i) \tag{21}$$

$$T_v = w_{vx} \cdot x_t + w_{vh} \cdot h_{t-1} + b_v \tag{22}$$

$$R_v = \mathbb{T}(T_v) \tag{23}$$

$$T_o = w_{ox} \cdot x_t + w_{oh} \cdot h_{t-1} + b_o \tag{24}$$

$$R_o = \mathbb{S}(T_o) \tag{25}$$

$$C_t = C_{t-1} R_f + R_i \cdot R_v \tag{26}$$

$$h_t = R_o \cdot \mathbb{T}(C_t) \tag{27}$$

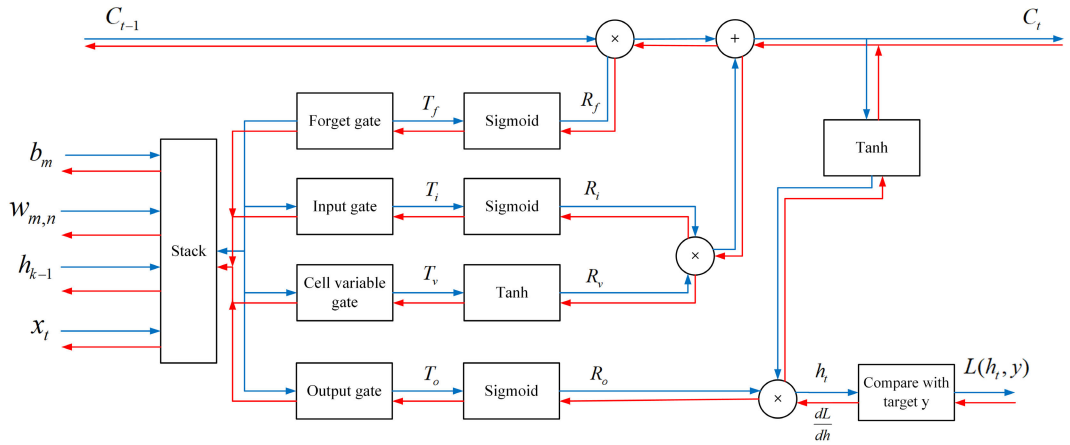

FIGURE 3. Structural representation of the LSTM model used.

where h_{t-1} is the previous state hidden vector, $X(t)$ is the input vector, b is the bias and w is the weight for each gate respectively.

$$L(h, y) = \frac{1}{2m}\sum_{m=1}^{m}(|h - y|^2) \tag{28}$$

where y is the target output and $h(x)$ is the predicted output.

2) BACKWARD PROPAGATION

Deriving the gradient through backward propagation through time at time stamp t using the chain rule is given below. The gradient passed down by the LSTM cell is:

$$e = \frac{dL}{dh_t} = h_t - y \tag{29}$$

The gradient with respect to the output gate

$$dR_o = \frac{dL}{dh_t} \cdot \frac{dh}{dR_o} = e \cdot \mathbb{T}(c_t) \tag{30}$$

The gradient with respect to c_t:

$$dc = \frac{dL}{dh_t} \cdot \frac{dh}{dc} = e \cdot R_o \cdot (1 - \mathbb{T}^2(c_t)) \tag{31}$$

The gradient with respect to i:

$$di = \frac{dL}{dc} \cdot \frac{dc}{di} = e \cdot R_v \cdot R_o \cdot (1 - \mathbb{T}^2(c_t)) \tag{32}$$

The gradient with respect to v:

$$dv = \frac{dL}{dc} \cdot \frac{dc}{dv} = e \cdot R_i \cdot R_o \cdot (1 - \mathbb{T}^2(c_t)) \tag{33}$$

The gradient with respect to f:

$$df = \frac{dL}{dc} \cdot \frac{dc}{dc_{t-1}} = e \cdot ct - 1 \cdot R_o \cdot (1 - \mathbb{T}^2(c_t)) \tag{34}$$

The gradient with respect to c_{t-1}:

$$dc_{t-1} = \frac{dL}{dc} \cdot \frac{dc}{dc_{t-1}} = e \cdot R_f \cdot R_o \cdot (1 - \mathbb{T}^2(c_t)) \tag{35}$$

The gradients with respect to weights and biases:

$$dw_{ox} = e \cdot \mathbb{T}(c_t) \cdot \mathbb{S}(T_O) \cdot (1 - \mathbb{S}(T_O)) \cdot x_t \tag{36}$$

$$dw_{oh} = e \cdot \mathbb{T}(c_t) \cdot \mathbb{S}(T_O) \cdot (1 - \mathbb{S}(T_O)) \cdot h_{t-1} \tag{37}$$

$$db_o = e \cdot \mathbb{T}(c_t) \cdot \mathbb{S}(T_O) \cdot (1 - \mathbb{S}(T_O)) \tag{38}$$

$$dw_{fx} = e \cdot R_o \cdot (1 - \mathbb{T}^2(c_t)) \cdot c_{t-1} \cdot \mathbb{S}(T_f) \cdot (1 - \mathbb{S}(T_f)) \cdot x_t \tag{39}$$

$$dw_{fh} = e \cdot R_o \cdot (1 - \mathbb{T}^2(c_t)) \cdot c_{t-1} \cdot \mathbb{S}(T_f) \cdot (1 - \mathbb{S}(T_f)) \cdot h_{t-1} \tag{40}$$

$$db_f = e \cdot R_o \cdot (1 - \mathbb{T}^2(c_t)) \cdot c_{t-1} \cdot \mathbb{S}(T_f) \cdot (1 - \mathbb{S}(T_f)) \tag{41}$$

$$dw_{ix} = e \cdot R_o \cdot (1 - \mathbb{T}^2(c_t)) \cdot R_i \cdot \mathbb{S}(T_i) \cdot (1 - \mathbb{S}(T_i)) \cdot x_t \tag{42}$$

$$dw_{ih} = e \cdot R_o \cdot (1 - \mathbb{T}^2(c_t)) \cdot R_i \cdot \mathbb{S}(T_i) \cdot (1 - \mathbb{S}(T_i)) \cdot h_{t-1} \tag{43}$$

$$db_i = e \cdot R_o \cdot (1 - \mathbb{T}^2(c_t)) \cdot R_i \cdot \mathbb{S}(T_i) \cdot (1 - \mathbb{S}(T_i)) \tag{44}$$

$$dw_{vx} = e \cdot R_o \cdot (1 - \mathbb{T}^2(c_t)) \cdot R_v \cdot \mathbb{S}(T_v) \cdot (1 - \mathbb{S}(T_v)) \cdot x_t \tag{45}$$

$$dw_{vh} = e \cdot R_o \cdot (1 - \mathbb{T}^2(c_t)) \cdot R_v \cdot \mathbb{S}(T_v) \cdot (1 - \mathbb{S}(T_v)) \cdot h_{t-1} \tag{46}$$

$$db_v = e \cdot R_o \cdot (1 - \mathbb{T}^2(c_t)) \cdot R_v \cdot \mathbb{S}(T_v) \cdot (1 - \mathbb{S}(T_v)) \tag{47}$$

The updates of weights and biases achieved through backward propagation are given by the following equations:

$$w_{mn} = w_{mn} - dw_{mn} \tag{48}$$

$$b_m = b_m - db_m \tag{49}$$

where m represents o, f, i, v and n represents x_t, h_{t-1} respectively.

IV. RESULTS AND DISCUSSIONS

The complementary cumulative distribution function (CCDF) and probability density function (PDF) of stochastic data usually provide convincing evidence by determining key

parameters such as the frequency of occurrence, mean, standard deviation and other statistical information embedded in the data. To determine the CCDFs and PDFs from actual measurements, we have used rain data collected using a disdrometer over a period of four years and 10 months data in South Korea and Ethiopia, respectively. Only the rainfall intensities and signal level data with values different from zero were used and processed to determine the statistical distributions. The actual received signal level and rainfall were used as inputs and targets for training and validation of the deep learning. The statistical distributions (CCDF and PDF) of the rainfall rate generated using deep learning (ANN and LSTM) techniques were compared with the actual rainfall measurements.

A. COMPLEMENTARY CUMULATIVE DISTRIBUTION FUNCTION (CCDF) COMPARISON OF DEEP LEARNING BASED GENERATED RAIN WITH MEASURED RAINFALL

In radio network planning, the CCDF is an important tool for determining the link budget availability indices in horizontal and slant links designs. The availability indices usually considered in link budget planning are 99.99 % or 0.01% of the time exceedance of the annual rainfall distribution [59], [60]. However, based on the severity of the rainfall conditions at a particular site 99%, 99.9%, and 99.999% of time exceedance also considered for the fade threshold evaluation of link budgets.

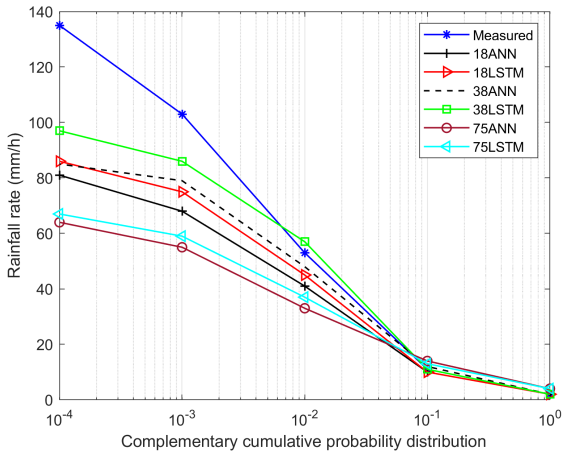

FIGURE 4. Comparison of complementary cumulative rainfall distribution functions generated by ANN and LSTM models and actual measurements over horizontal links in South Korea.

Fig. 4 presents the CCDF comparison of rainfall intensity obtained from measured and generated rain rate data using the proposed deep learning techniques for terrestrial line-of-sight links in Icheon, South Korea. From Fig. 4, it is clear that the CCDF generated using LSTM at an operating frequency of 38 GHz gives the best fit to the measured data compared to the generated CCDF at 18 GHz and 75 GHz frequencies. Also the CCDF generated using LSTM gives better fit to the measured data compared to the generated CCDF using ANN.

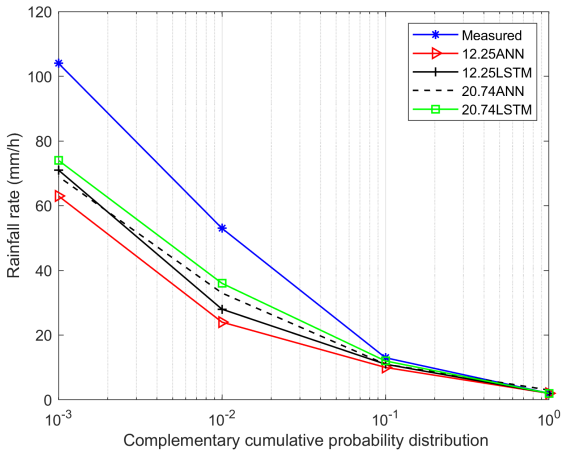

FIGURE 5. Comparison of complementary cumulative rainfall distribution functions generated by ANN and LSTM models and actual measurements over satellite links in South Korea.

Fig. 5 shows the CCDF comparison of rainfall rates for satellite links in South Korea. From Fig. 5, it is observed that the CCDF obtained from the generated rainfall data using deep learning underestimates the measured rainfall rate CCDF. This is owing to the fact that the slant link radio wave signals penetrate the whole troposphere, which contains different no-rain atmospheric elements. Therefore, the correlation between rainfall and rain-induced attenuation is not strong in satellite links compared to terrestrial links.

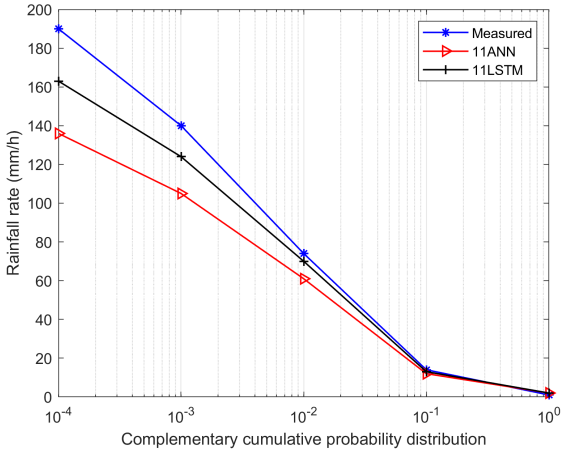

FIGURE 6. Comparison of complementary cumulative rainfall distribution functions generated by ANN and LSTM models and actual measurements over horizontal links in Ethiopia.

Fig. 6 shows the rainfall rate CCDF of the microwave link in Ethiopia between Addis Ababa and Furi at 11 GHz carrier frequency over a link distance of 16.4 km. From Fig. 6, it is observed that the CCDF from the LSTM-generated rainfall data provides the best fit to the actual rainfall measurement.

This is due to the longer link length; the longer the link, the higher the rain attenuation, which increases the total attenuation of the link and provides a more suitable rainfall prediction.

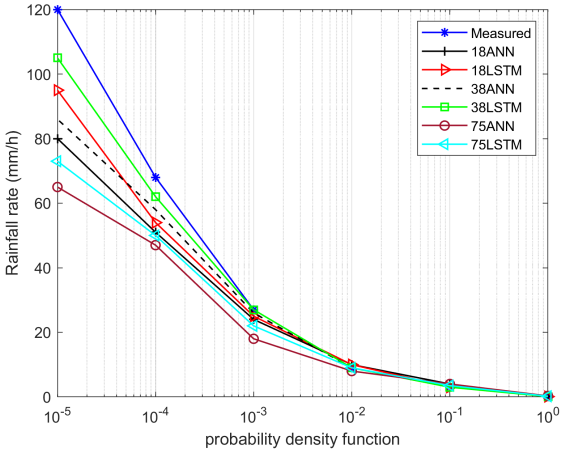

FIGURE 7. Probability density function comparison of rainfall rate generated by ANN and LSTM models and actual measurements over horizontal links in South Korea.

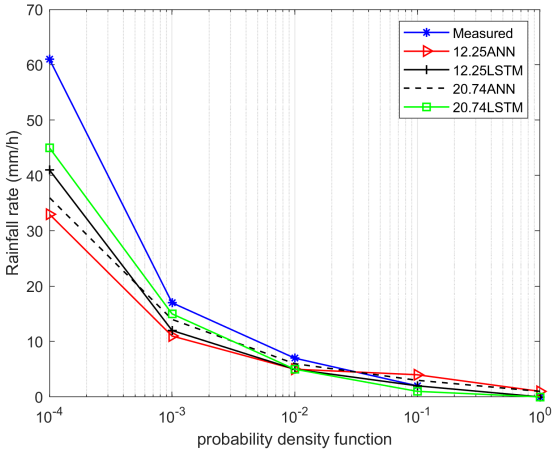

FIGURE 8. Probability density function comparison of rainfall rate generated by ANN and LSTM models and actual measurements over satellite links in South Korea.

B. PROBABILITY DENSITY FUNCTION COMPARISON OF GENERATED WITH ACTUAL RAINFALL RATE

Figs. 7,8,9 show the PDFs of actual rainfall data recorded and generated rain data using the ANN and LSTM for the terrestrial and satellite links in South Korea, and terrestrial microwave link in Ethiopia, respectively. From Fig. 7, which shows the terrestrial links in South Korea, it is clearly seen that the generated LSTM model PDF gives a better fit to the actual PDF compare to the PDF generated from the ANN model at the same operating frequency. In addition, the 38 GHz carrier frequency gives a better fit to the measured

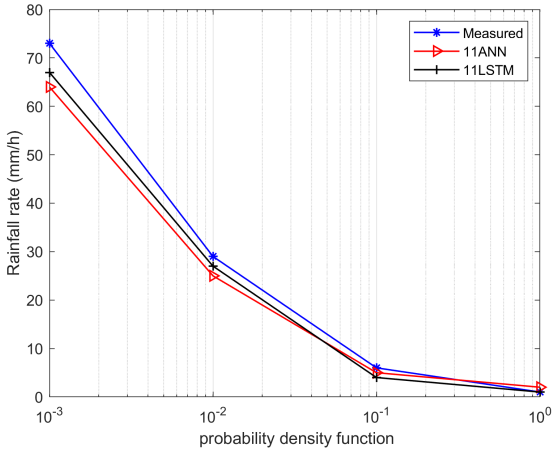

FIGURE 9. Probability density function comparison of rainfall rate generated by ANN and LSTM models and actual measurements over microwave link in Ethiopia.

rainfall PDF. This is owing to the fact that higher frequency signals are more sensitive to rainfall. However, the rain rate generated at E-band (75-GHz) gives poorer fit to the measured rainfall rate than 38 GHz owing to its lower wavelength compared to the raindrop diameter.

Fig. 8 shows the PDF of rainfall at the slant link in South Korea, where the generated PDF distribution of rainfall over the satellite link gives less closer than the measurement compared to the terrestrial link. This is because of the impact of the complex non-rainy atmospheric elements, such as clouds, gasses and turbulence, through which the satellite link signals propagate in the troposphere.

Fig. 9 shows the measured and generated PDF distribution in Ethiopia. The results show a well-fitted distribution due to longer link length. The longer the link distance, the greater is the attenuation due to rain. In addition, LSTM-generated rainfall gives a better fit to the measured PDF compared to the ANN equivalent.

In general, the rainfall rates generated from the terrestrial links provide better fit than the slant links. The links with a lower frequency and shorter link length have a smaller attenuation under the same weather conditions, which may influence the rainfall monitoring results. The LSTM model gives better predictions than the ANN model for the same link distance and operating frequencies.

C. RAIN RATE GENERATION USING DEEP LEARNING

Fig. 10 and Fig. 11 show the measured and sample-generated rainfall rate events against received signal levels at 38 GHz of the terrestrial link using ANN and LSTM learning models, respectively. Rainfall events were recorded on July 6th, 2016 in South Korea. It is clearly observed that as the received signal level (RSL) values decrease, the corresponding rainfall rate values increase, that is, high attenuation of the signal power indicates higher rainfall. The figures illustrate that the measured and predicted rainfall rates are well fitted up to 50 mm/h and undermine the measured rainfall rate above

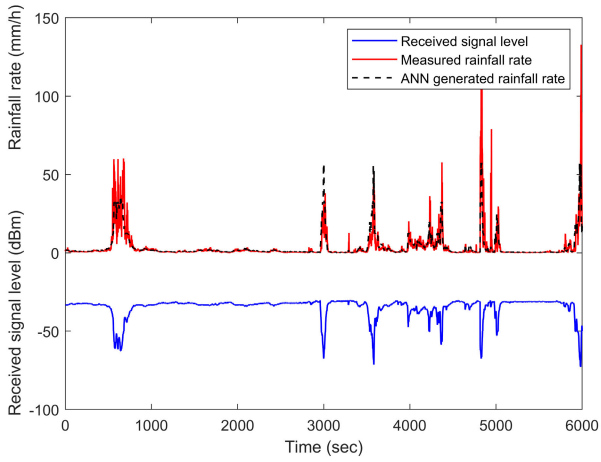

FIGURE 10. Time series rainfall from artificial neural network (ANN) generation and actual rain data against time variation of measured received signal level along the path.

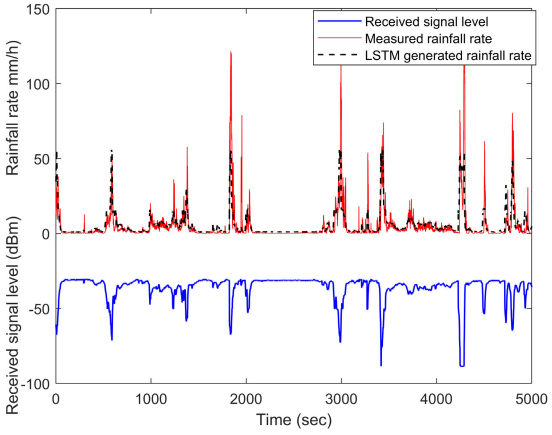

FIGURE 11. Temporal variation of long short-term memory (LSTM) generated and measured rainfall rate with respect to the variation of measured received signal level along the path.

50 mm/h. The performance evaluations of the two models are presented in Table 2.

D. PERFORMANCE ANALYSIS

To evaluate the performances of the ANN and LSTM models, we implemented the goodness of fit functions, which measure how well the generated rain data from the models fit the measured rainfall data. The goodness of fit functions are: the coefficient of determination (R^2), root-mean-square error ($RMSE$), and correlation coefficient (CC), respectively. They are considered as evaluation metrics, and their corresponding equations are defined in [1] as follows:

$$RMSE = \sqrt{\frac{1}{N}\sum_{i=1}^{N}(R_p(i) - R_m(i))^2} \tag{50}$$

TABLE 2. Performance evaluation metrics for ANN and LSTM models at different links frequencies and locations.

Links (GHz)	LSTM			ANN		
	RMSE	R^2	CC	RMSE	R^2	CC
18	7.2	0.946	0.981	8.3	0.925	0.98
38	5.4	0.98	0.994	5.4	0.97	0.99
75	10.3	0.89	0.93	12.1	0.86	0.92
12.25	17.2	0.62	0.884	20.1	0.59	0.88
20.74	15.6	0.73	0.91	16.8	0.68	0.9
11	8.4	0.81	0.92	9.1	0.77	0.91

$$R^2 = 1 - \frac{\sum_{i=1}^{N}(R_m(i) - R_p(i))^2}{\sum_{i=1}^{N}(R_p(i) - \overline{R_m})^2} \tag{51}$$

$$CC = \frac{(R_p(i) - \overline{R_p})(R_m(i) - \overline{R_m})}{\sqrt{\sum_{i=1}^{N}(R_p(i) - \overline{R_p})^2}\sqrt{\sum_{i=1}^{N}(R_m(i) - \overline{R_m})^2}} \tag{52}$$

where R_p and R_m are the predicted and measured rainfall rate, respectively, whereas $\overline{R_p}$ and $\overline{R_m}$ are the mean values of predicted and measured rainfall rate, respectively.

Table 2 tabulates the performance evaluation metrics on different links operating in South Korea and Ethiopia at various operating frequencies for ANN and LSTM models. The calculated performance results in terms of $RMSE$, R^2 and CC are valid and show the LSTM over performs an ANN model over all links.

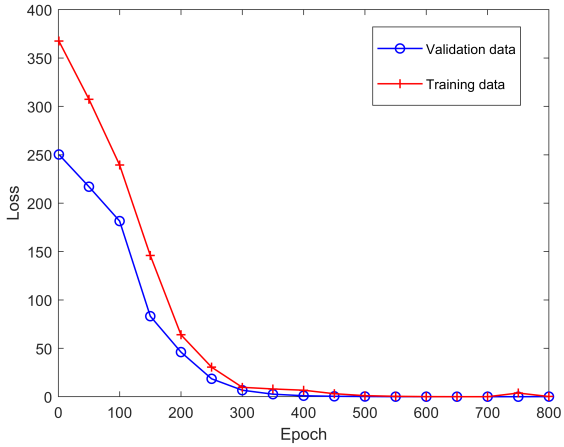

FIGURE 12. Loss function during training time of terrestrial links at 38 GHz using ANN.

Fig. 12 and Fig. 13 show the loss functions of the ANN and LSTM network architectures, respectively, for the 38 GHz

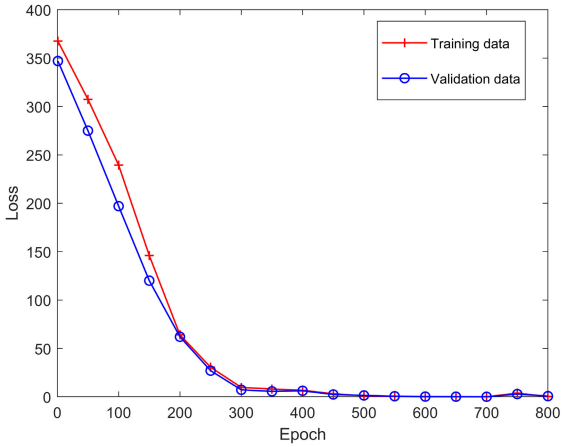

FIGURE 13. Loss function during training time of terrestrial links at 38-GHz using LSTM.

bands over a horizontal link in South Korea. The loss functions for the training dataset were much lower than those for the validation dataset. This indicates that the proposed deep learning networks do not overfit the training phase.

V. CONCLUSION

This study investigates the application of wireless telecommunication networks for monitoring rainfall rates in South Korea and Ethiopia. Explicitly, the aim of this study is to investigate the rainfall generation from terrestrial line-of-sight links at 18, 38, and 75 GHz operating frequencies, and from satellite links at 12.25 and 20.74 GHz frequency bands in South Korea. We also investigated results from a microwave link at 11 GHz in Ethiopia using a deep learning approach. Four years and ten months of measured received signal level and rainfall rate data were collected during the rainy season in South Korea and Ethiopia, respectively, and were used for training and validation of the ANN and LSTM models. We then compared the experimental results of rainfall rate distribution with the rainfall rate distribution generated from two deep learning models (ANN and LSTM). From the results, it is observed that the terrestrial links provide better predictions than satellite links because of the impact of non-rainy atmospheric factors through which the satellite link radio wave propagates, and the LSTM model outperforms the ANN model. In general, links with higher frequencies have higher rain attenuation than those with lower frequencies and are more appropriate for monitoring rainfall. However, the 38 GHz band is more accurate at higher rainfall rates than the 75 GHz band because the wavelength of the 75 GHz band is shorter than the raindrop size. Although more experiments are needed to validate these conclusions, the opportunistic use of extensively distributed wireless telecommunication networks has significant potential for global rainfall monitoring. In general, the findings will benefit the area of hydrometeorology, agriculture, climate monitoring, and natural disaster warning at locations where rain data are insufficient or unavailable.

REFERENCES

[1] M. Xian, X. Liu, M. Yin, K. Song, S. Zhao, and T. Gao, "Rainfall monitoring based on machine learning by Earth-space link in the ku band," *IEEE J. Sel. Topics Appl. Earth Observ. Remote Sens.*, vol. 13, pp. 3656–3668, 2020, doi: 10.1109/jstars.2020.3004375.

[2] M. F. McCabe, M. Rodell, D. E. Alsdorf, D. G. Miralles, R. Uijlenhoet, W. Wagner, A. Lucieer, R. Houborg, N. E. C. Verhoest, T. E. Franz, J. Shi, H. Gao, and E. F. Wood, "The future of Earth observation in hydrology," *Hydrol. Earth Syst. Sci.*, vol. 21, no. 7, pp. 3879–3914, Jul. 2017, doi: 10.5194/hess-21-3879-2017.

[3] O. Goldshtein, H. Messer, and A. Zinevich, "Rain rate estimation using measurements from commercial telecommunications links," *IEEE Trans. Signal Process.*, vol. 57, no. 4, pp. 1616–1625, Apr. 2009, doi: 10.1109/tsp.2009.2012554.

[4] C. Lorenz and H. Kunstmann, "The hydrological cycle in three state-of-the-art reanalyses: Intercomparison and performance analysis," *J. Hydrometeorology*, vol. 13, no. 5, pp. 1397–1420, Oct. 2012, doi: 10.1175/jhm-d-11-088.1.

[5] K. Song, X. Liu, and T. Gao, "Real-time rainfall estimation using microwave links: A case study in east China during the plum rain season in 2020," *Sensors*, vol. 21, no. 3, p. 858, Jan. 2021, doi: 10.3390/s21030858.

[6] F. Fenicia, L. Pfister, D. Kavetski, P. Matgen, J.-F. Iffly, L. Hoffmann, and R. Uijlenhoet, "Microwave links for rainfall estimation in an urban environment: Insights from an experimental setup in Luxembourg-City," *J. Hydrol.*, vols. 464–465, pp. 69–78, Sep. 2012, doi: 10.1016/j.jhydrol.2012.06.047.

[7] M.-S. Kim and B. Kwon, "Rainfall detection and rainfall rate estimation using microwave attenuation," *Atmosphere*, vol. 9, no. 8, p. 287, Jul. 2018, doi: 10.3390/atmos9080287.

[8] F. D. Diba, T. J. Afullo, and A. A. Alonge, "Rainfall rate and attenuation performance analysis at microwave and millimeter bands for the design of terrestrial line-of-sight radio links in Ethiopia," *SAIEE Afr. Res. J.*, vol. 107, no. 3, pp. 177–186, Sep. 2016, doi: 10.23919/saiee.2016.8532241.

[9] F. D. Diba and T. J. Afullo, "Estimation of rain attenuation over microwave and millimeter bands for terrestrial radio links in Ethiopia," in *Proc. AFRICON*, Sep. 2015, pp. 1–5, doi: 10.1109/afrcon.2015.7332053.

[10] F. D. Diba, T. J. Afullo, and A. A. Alonge, "Time series rainfall spike modelling from Markov chains and queueing theory approach for rainfall attenuation over terrestrial and Earth-space radio wave propagation in Jimma, Ethiopia," in *Proc. Prog. Electromagn. Res. Symp. (PIERS)*, Aug. 2016, pp. 4991–4995, doi: 10.1109/piers.2016.7735815.

[11] M. A. Samad, F. D. Diba, and D.-Y. Choi, "A survey of rain attenuation prediction models for terrestrial links—Current research challenges and state-of-the-art," *Sensors*, vol. 21, no. 4, p. 1207, Feb. 2021, doi: 10.3390/s21041207.

[12] D. Atlas and C. W. Ulbrich, "Path-and area-integrated rainfall measurement by microwave attenuation in the 1–3 cm band," *J. Appl. Meteorol.*, vol. 16, no. 11, pp. 1322–1331, 1977. [Online]. Available: https://journals.ametsoc.org/view/journals/apme/16/12/1520-0450_1977_016_1322_paairm_2_0_co_2.xml

[13] R. Olsen, D. Rogers, and D. Hodge, "The aR^b relation in the calculation of rain attenuation," *IEEE Trans. Antennas Propag.*, vol. AP-26, no. 2, pp. 318–329, Mar. 1978, doi: 10.1109/tap.1978.1141845.

[14] S. Krämer, H.-R. Verworn, and A. Redder, "Improvement of X-band radar rainfall estimates using a microwave link," *Atmos. Res.*, vol. 77, nos. 1–4, pp. 278–299, Sep. 2005, doi: 10.1016/j.atmosres.2004.10.028.

[15] H. Messer, A. Zinevich, and A. Pinhas, "Environmental monitoring by wireless communication networks," *Science*, vol. 312, no. 5774, p. 713, 2006, doi: 10.1126/science.1120034.

[16] A. Overeem, H. Leijnse, and R. Uijlenhoet, "Measuring urban rainfall using microwave links from commercial cellular communication networks," *Water Resour. Res.*, vol. 47, no. 12, Dec. 2011, Art. no. W12 505, doi: 10.1029/2010wr010350.

[17] M. Graf, C. Chwala, J. Polz, and H. Kunstmann, "Rainfall estimation from a german-wide commercial microwave link network: Optimized processing and validation for 1 year of data," *Hydrol. Earth Syst. Sci.*, vol. 24, no. 6, pp. 2931–2950, Jun. 2020, doi: 10.5194/hess-24-2931-2020.

[18] A. Overeem, H. Leijnse, and R. Uijlenhoet, "Two and a half years of country-wide rainfall maps using radio links from commercial cellular telecommunication networks," *Water Resour. Res.*, vol. 52, no. 10, pp. 8039–8065, Oct. 2016, doi: 10.1002/2016wr019412.

[19] J. Polz, C. Chwala, M. Graf, and H. Kunstmann, "Rain event detection in commercial microwave link attenuation data using convolutional neural networks," *Atmos. Meas. Techn.*, vol. 13, no. 7, pp. 3835–3853, Jul. 2020, doi: 10.5194/amt-13-3835-2020.

[20] G. Smiatek, F. Keis, C. Chwala, B. Fersch, and H. Kunstmann, "Potential of commercial microwave link network derived rainfall for river runoff simulations," *Environ. Res. Lett.*, vol. 12, no. 3, Mar. 2017, Art. no. 034026, doi: 10.1088/1748-9326/aa5f46.

[21] J. Pastorek, M. Fencl, J. Rieckermann, and V. Bareš, "Commercial microwave links for urban drainage modelling: The effect of link characteristics and their position on runoff simulations," *J. Environ. Manage.*, vol. 251, Dec. 2019, Art. no. 109522, doi: 10.1016/j.jenvman.2019.109522.

[22] A. Doumounia, M. Gosset, F. Cazenave, M. Kacou, and F. Zougmore, "Rainfall monitoring based on microwave links from cellular telecommunication networks: First results from a West African test bed," *Geophys. Res. Lett.*, vol. 41, no. 16, pp. 6016–6022, Aug. 2014, doi: 10.1002/2014gl060724.

[23] S. Kun, G. Tai-Chang, L. Xi-Chuan, Y. Min, and X. Yang, "Method and experiment of rainfall intensity inversion using a microwave link based on support vector machine," *Acta Phys. Sinica*, vol. 64, no. 24, 2015, Art. no. 244301, doi: 10.7498/aps.64.244301.

[24] G. Tai-Chang, S. Kun, L. Xi-Chuan, Y. Min, L. Lei, and J. Shi-Tai, "Research on the method and experiment of path rainfall intensity inversion using a microwave link," *Acta Phys. Sinica*, vol. 64, no. 17, 2015, Art. no. 174301, doi: 10.7498/aps.64.174301.

[25] A. R. Rahimi, A. R. Holt, G. J. G. Upton, S. Krämer, A. Redder, and H.-R. Verworn, "Attenuation calibration of an X-band weather radar using a microwave link," *J. Atmos. Ocean. Technol.*, vol. 23, no. 3, pp. 395–405, Mar. 2006, doi: 10.1175/jtech1855.1.

[26] J. Shi-Tai, G. Tai-Chang, L. Xi-Chuan, L. Lei, and L. Zhi-Tian, "Investigation of the inversion of rainfall field based on microwave links," *Acta Phys. Sinica*, vol. 62, no. 15, 2013, Art. no. 154303, doi: 10.7498/aps.62.154303.

[27] C. Han, J. Huo, Q. Gao, G. Su, and H. Wang, "Rainfall monitoring based on next-generation millimeter-wave backhaul technologies in a dense urban environment," *Remote Sens.*, vol. 12, no. 6, p. 1045, Mar. 2020, doi: 10.3390/rs12061045.

[28] L. Barthès and C. Mallet, "Rainfall measurement from the opportunistic use of an Earth–space link in the ku band," *Atmos. Meas. Techn.*, vol. 6, no. 8, pp. 2181–2193, Aug. 2013, doi: 10.5194/amt-6-2181-2013.

[29] X. Shen, D. D. Huang, B. Song, C. Vincent, and R. Togneri, "3-D tomographic reconstruction of rain field using microwave signals from LEO satellites: Principle and simulation results," *IEEE Trans. Geosci. Remote Sens.*, vol. 57, no. 8, pp. 5434–5446, Aug. 2019, doi: 10.1109/tgrs.2019.2899391.

[30] M.-H. Xian, X.-C. Liu, M. Yin, K. Song, and T.-C. Gao, "Inversion of vertical rainfall field based on Earth-space links," *Acta Phys. Sinica*, vol. 69, no. 2, 2020, Art. no. 024301, doi: 10.7498/aps.69.20191232.

[31] H. Messer, "Capitalizing on cellular technology—Opportunities and challenges for near ground weather monitoring," *Environments*, vol. 5, no. 7, p. 73, Jun. 2018, doi: 10.3390/environments5070073.

[32] M. Schleiss and A. Berne, "Identification of dry and rainy periods using telecommunication microwave links," *IEEE Geosci. Remote Sens. Lett.*, vol. 7, no. 3, pp. 611–615, Jul. 2010, doi: 10.1109/lgrs.2010.2043052.

[33] M. Fencl, M. Dohnal, P. Valtr, M. Grabner, and V. Bareš, "Atmospheric observations with E-band microwave links—Challenges and opportunities," *Atmos. Meas. Techn.*, vol. 13, no. 12, pp. 6559–6578, Dec. 2020, doi: 10.5194/amt-13-6559-2020.

[34] C. Chwala, A. Gmeiner, W. Qiu, S. Hipp, D. Nienaber, U. Siart, T. Eibert, M. Pohl, J. Seltmann, J. Fritz, and H. Kunstmann, "Precipitation observation using microwave backhaul links in the alpine and pre-alpine region of Southern Germany," *Hydrol. Earth Syst. Sci.*, vol. 16, no. 8, pp. 2647–2661, Aug. 2012, doi: 10.5194/hess-16-2647-2012.

[35] Z. Wang, M. Schleiss, J. Jaffrain, A. Berne, and J. Rieckermann, "Using Markov switching models to infer dry and rainy periods from telecommunication microwave link signals," *Atmos. Meas. Techn.*, vol. 5, no. 7, pp. 1847–1859, Jul. 2012, doi: 10.5194/amt-5-1847-2012.

[36] V. Đorević, O. Pronić-Rančić, Z. Marinković, M. Milijić, V. Marković, U. Siart, C. Chwala, and H. Kunstmann, "New method for detection of precipitation based on artificial neural networks," *Microw. Rev.*, vol. 19, no. 2, pp. 1–6, 2013.

[37] J. Ostrometzky and H. Messer, "Dynamic determination of the baseline level in microwave links for rain monitoring from minimum attenuation values," *IEEE J. Sel. Topics Appl. Earth Observ. Remote Sens.*, vol. 11, no. 1, pp. 24–33, Jan. 2018, doi: 10.1109/jstars.2017.2752902.

[38] Y. LeCun, Y. Bengio, and G. Hinton, "Deep learning," *Nature*, vol. 521, no. 7553, pp. 436–444, May 2015, doi: 10.1038/nature14539.

[39] K. V. Mishra, A. Gharanjik, M. B. Shankar, and B. Ottersten, "Deep learning framework for precipitation retrievals from communication satellites," in *Proc. Eur. Conf. Radar Meteorol. Hydrol.*, Ede-Wageningen, The Netherlands, Jun. 2018, p. 23.

[40] H. V. Habi and H. Messer, "Wet-dry classification using LSTM and commercial microwave links," in *Proc. IEEE 10th Sensor Array Multichannel Signal Processing Workshop (SAM)*, Sheffield, U.K., Jul. 2018, pp. 149–153, doi: 10.1109/sam.2018.8448679.

[41] F. Kratzert, D. Klotz, C. Brenner, K. Schulz, and M. Herrnegger, "Rainfall-runoff modelling using long-short-term-memory (LSTM) networks," *Hydrol. Earth Syst. Sci.*, vol. 22, no. 11, pp. 6005–6022, May 2018, doi: 10.5194/hess-2018-247.

[42] C. Hu, Q. Wu, H. Li, S. Jian, N. Li, and Z. Lou, "Deep learning with a long short-term memory networks approach for rainfall-runoff simulation," *Water*, vol. 10, no. 11, p. 1543, Oct. 2018, doi: 10.3390/w10111543.

[43] S. Shrestha and D.-Y. Choi, "Rain attenuation study over an 18 GHz terrestrial microwave link in South Korea," *Int. J. Antennas Propag.*, vol. 2019, pp. 1–16, Mar. 2019, doi: 10.1155/2019/1712791.

[44] F. D. Diba, M. A. Samad, and D.-Y. Choi, "The effects of rain on terrestrial links at K, Ka and E-bands in South Korea: Based on supervised learning," *IEEE Access*, vol. 9, pp. 9345–9355, 2021, doi: 10.1109/access.2021.3049825.

[45] S. Shrestha and D.-Y. Choi, "Characterization of rain specific attenuation and frequency scaling method for satellite communication in South Korea," *Int. J. Antennas Propag.*, vol. 2017, pp. 1–16, 2017, doi: 10.1155/2017/8694748.

[46] P. Thiennviboon and S. Wisutimateekorn, "Rain attenuation prediction modeling for Earth-space links using artificial neural networks," in *Proc. 16th Int. Conf. Electr. Eng./Electron., Comput., Telecommun. Inf. Technol. (ECTI-CON)*, Jul. 2019, pp. 10–13, doi: 10.1109/ECTI-CON47248.2019.8955194.

[47] S. Theodoridis, *Machine Learning: A Bayesian and Optimization Perspective*. Cambridge, MA, USA: Academic, 2015.

[48] A. Aguinaga, X. Luo, V. Hidalgo, E. Cando, and F. Llulluna, "A feed-forward backpropagation neural network method for remaining useful life prediction of francis turbines," in *Proc. 3rd World Congr. Mech., Chem., Mater. Eng.*, Jun. 2017, pp. 8–10, doi: 10.11159/icmie17.126.

[49] A. Gharanjik, K. V. Mishra, B. S. M. R., and B. Ottersten, "Learning-based rainfall estimation via communication satellite links," in *Proc. IEEE Stat. Signal Process. Workshop (SSP)*, Jun. 2018, pp. 10–13, doi: 10.1109/SSP.2018.8450726.

[50] J. Heaton, *Introduction to Neural Networks With Java*. Chesterfield, MO, USA: Heaton Research, 2008.

[51] A. Ghatak, *Deep Learning With R*. Singapore: Springer, 2019, doi: 10.1007/978-981-13-5850-0.

[52] O. Irsoy and E. Alpaydın, "Unsupervised feature extraction with autoencoder trees," *Neurocomputing*, vol. 258, pp. 63–73, Oct. 2017, doi: 10.1016/j.neucom.2017.02.075.

[53] H. Musafer, A. Abuzneid, M. Faezipour, and A. Mahmood, "An enhanced design of sparse autoencoder for latent features extraction based on trigonometric simplexes for network intrusion detection systems," *Electronics*, vol. 9, no. 2, p. 259, Feb. 2020, doi: 10.3390/electronics9020259.

[54] K. Abhishek, A. Kumar, R. Ranjan, and S. Kumar, "A rainfall prediction model using artificial neural network," in *Proc. IEEE Control Syst. Graduate Res. Colloq.*, Jul. 2012, pp. 16–17, doi: 10.1109/ICSGRC.2012.6287140.

[55] S. Hochreiter and J. Schmidhuber, "Long short-term memory," *Neural Comput.*, vol. 9, no. 8, pp. 1735–1780, Nov. 1997, doi: 10.1162/neco.1997.9.8.1735.

[56] C. Olah. (2015). *Understanding LSTM Networks*. [Online]. Available: http://colah.github.io/posts/2015-08-Understanding-LSTMs/

[57] Z. C. Lipton, J. Berkowitz, and C. Elkan, "A critical review of recurrent neural networks for sequence learning," Tech. Rep., 2015. [Online]. Available: https://arxiv.org/abs/1506.00019

[58] F. A. Gers and J. Schmidhuber, "Recurrent nets that time and count," in *Proc. IEEE-INNS-ENNS Int. Joint Conf. Neural Netw. IJCNN Neural Comput., New Challenges Perspect. New Millennium*, Jul. 2000, pp. 189–194, doi: 10.1109/IJCNN.2000.861302.

[59] A. A. Alonge and T. J. Afullo, "Rainfall time series synthesis from queue scheduling of rain event fractals over radio links," *Radio Sci.*, vol. 50, no. 12, pp. 1209–1224, Dec. 2015, doi: 10.1002/2015rs005791.

[60] F. Moupfouma, "More about rainfall rates and their prediction for radio systems engineering," *IEE Proc. H Microw., Antennas Propag.*, vol. 134, no. 6, p. 527, 1987, doi: 10.1049/ip-h-2.1987.0106.

FEYISA DEBO DIBA received the B.Sc. degree in electrical engineering from Arba Minch University, Arba Minch, Ethiopia, in 2006, the M.Sc. degree in communication systems engineering from Addis Ababa University, Addis Ababa, Ethiopia, in 2010, and the Ph.D. degree in electronic engineering from the University of Kwazulu-Natal, Durban, South Africa, in 2017. He is currently a Postdoctoral Fellow with Chosun University, Gwangju, South Korea. His research interests include radio wave propagation measurements and modeling, cellular network planning, and optimization for 5G and beyond.

MD ABDUS SAMAD (Graduate Student Member, IEEE) is currently pursuing the Ph.D. degree in information and communication engineering with Chosun University, Gwangju, South Korea. Since 2013, he has been an Assistant Professor with the Department of Electronic and Telecommunication Engineering, International Islamic University Chittagong, Chattogram, Bangladesh. His research interests include signal processing, antenna design, electromagnetic wave propagation, applications of artificial neural networks and deep learning, and attenuation of millimeter-wave propagation by interference or atmospheric cause for 5G and beyond wireless networks.

JIWAN GHIMIRE received the B.S. degree in electronics and communication engineering from Tribhuvan University, Nepal, in 2010, and the M.S. degree from the Department of Electronics Engineering, Chosun University, Gwangju, South Korea, in 2019. He is currently working as a Research Assistant with the Department of Information and Communication Engineering, Chosun University. In Nepal, he had worked as a Software Engineer, a Knitting Machine Engineer, and a Textile Designer. His research interests include microwave and satellite communications, antenna design, UWB radar systems, and microwave imaging techniques.

DONG-YOU CHOI (Senior Member, IEEE) received the B.S., M.S., and Ph.D. degrees from the Department of Electronics Engineering, Chosun University, Gwangju, South Korea, in 1999, 2001, and 2004, respectively. Since 2006, he has been a Professor with the Department of Information and Communication Engineering, Chosun University. His research interests include rain attenuation, antenna design, wave propagation, and microwave and satellite communications. He is a member of KEES, IEEK, and KICS.